ANTIOXIDANTS & REDOX SIGNALING
Volume 14, Number 6, 2011

DOI: 10.1089/ars.2010.3417

FORUM REVIEW ARTICLE

Flavin Redox Switching of Protein Functions

Donald F. Becker, Weidong Zhu, and Michael A. Moxley

Abstract

Flavin cofactors impart remarkable catalytic diversity to enzymes, enabling them to participate in a broad array of biological processes. The properties of flavins also provide proteins with a versatile redox sensor that can be utilized for converting physiological signals such as cellular metabolism, light, and redox status into a unique functional output. The control of protein functions by the flavin redox state is important for transcriptional regulation, cell signaling pathways, and environmental adaptation. A significant number of proteins that have flavin redox switches are found in the Per-Arnt-Sim (PAS) domain family and include flavoproteins that act as photosensors and respond to changes in cellular redox conditions. Biochemical and structural studies of PAS domain flavoproteins have revealed key insights into how flavin redox changes are propagated to the surface of the protein and translated into a new functional output such as the binding of a target protein in a signaling pathway. Mechanistic details of proteins unrelated to the PAS domain are also emerging and provide novel examples of how the flavin redox state governs protein–membrane interactions in response to appropriate stimuli. Analysis of different flavin switch proteins reveals shared mechanistic themes for the regulation of protein structure and function by flavins. *Antioxid. Redox Signal.* 14, 1079–1091.

Introduction

Flavoenzymes are recognized for catalyzing a variety of reactions utilizing flavin mononucleotide (FMN) and flavin adenine dinculeotide (FAD) as noncovalently or covalently bound cofactors (18, 45). Flavins support one-electron and two-electron transfer processes involving the N(1), C(4a), and N(5) positions of the isoalloxazine ring system (18, 45). The types of reactions catalyzed by flavoenzymes include dehydrogenation, electron transfer, hydroxylation, dehalogenation, DNA repair, disulfide reduction, luminescence, and histone demethylation (17, 45). These chemical transformations provide important outcomes in numerous biological processes such as energy metabolism, amino acid metabolism, DNA synthesis, fatty acid metabolism, cholesterol, neuroactive compounds, chromatin remodeling, and bioremediation of polychlorinated aromatics (45). In addition to supporting diverse biochemical reactions, the flavin cofactor is sometimes employed to regulate protein function. In this role, the flavin redox state mediates protein interactions with other macromolecules such as effector/target proteins, membranes, and nucleic acids. The regulation of these macromolecular interactions by the flavin is important for various cellular processes such as circadian clocks, phototropism, transcriptional regulation, signal transduction, and cell motility (9, 15, 55).

The purpose of this review is to provide a survey of mechanistic details that have emerged in recent years concerning flavin-dependent regulation of proteins, also known as flavin redox switches. In flavin redox switches, an input signal changes the redox state of the bound flavin cofactor which is then converted into a new functional output as shown in Figure 1. The conversion of the input signal into a functional output involves a conformational change that is concomitant with a flavin redox change. Depending on the physiological environment and signaling pathway, the redox resting state of the flavin can be in the oxidized or reduced form. Input signals that cause reduction of the flavin may involve substrate binding and electron transfer to the flavin, electron reduction of the flavin by a physiological donor, or light-mediated reduction of the flavin. The reductive redox change is then transmitted to other domains in the protein to generate the desired functional output. The functional change can then be reversed by oxidation of the flavin. For some switches, strong evidence is available to show that they are reversible, while other switches may not necessarily be reversible.

This review highlights the proteins Vivid (VVD), NifL, pyruvate oxidase (POX), and proline utilization A (PutA) which are all flavin switch proteins with diverse functions and regulatory roles. These proteins were chosen because recent biochemical and structural studies of these flavin switch proteins have provided novel details into how cofactor reduction/modification leads to the propagation of conformational and functional changes (50, 69, 83, 90). Two of the

Department of Biochemistry, University of Nebraska-Lincoln, Lincoln, Nebraska.

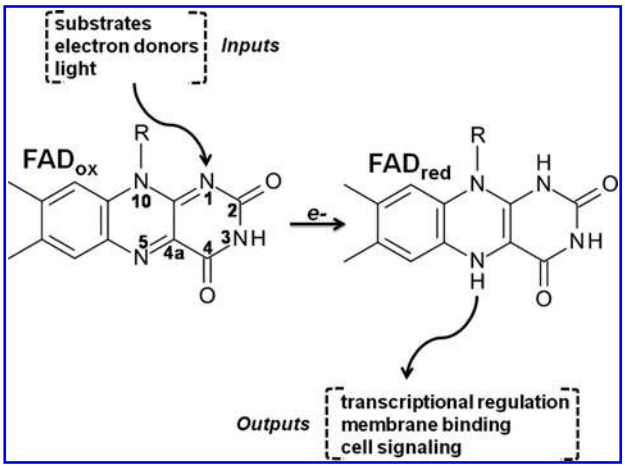

FIG. 1. Flavin redox switches. Various input signals can deliver a redox change to the flavin cofactor that results in the activation of a protein function. Examples of regulated output functions include the binding of a target/effector protein in a cell signaling cascade, membrane binding and intracellular localization, and transcriptional regulation.

proteins, VVD and NifL, contain a flavin-binding Per Arnt Sim (PAS) domain (64, 66). PAS domains are involved in numerous signaling pathways that respond to light, energy, redox status, and small molecules and besides flavin can bind different redox cofactors that include heme, 4Fe–4S clusters, and 4-hydroxycinnamic acid (26, 72). VVD is a light sensor protein important for setting circadian rhythms and is a member of the LOV (light, oxygen, and voltage) protein family which is a subset of the larger PAS domain family (64, 90). NifL is not a light sensor but rather responds to cellular redox status to control nitrogenase production in response to environmental oxygen (28). POX and PutA have structures unrelated to PAS domains and respond to intracellular concentrations of substrates that direct their movement from the cytosol to the membrane (50). PutA is unique in that it switches from a DNA-binding protein to a membrane-bound enzyme depending on proline availability (85). A key mechanistic feature for the flavin redox switch in the aforementioned proteins is the hydrogen bond network that allows communication between the N(1) and N(5) atoms of the flavin and the regulatory/functional domains (29). Redox signal transmission is best understood for the flavin PAS domain proteins due to biochemical studies and new crystal structures of PAS domains in the oxidized and light-reduced states (90).

Vivid (Light Sensor) Protein

Light-induced signaling is a fascinating phenomenon that occurs in a wide range of organisms (36, 40). Proper responses to light are necessary for organisms to survive in changing environmental conditions (36). The LOV (light, oxygen, and voltage), BLUF (blue light sensing using flavin), and cryptochromes represent three different types of photoreceptors that use flavin for capturing photoenergy and converting the light signal into an output that regulates processes such as phototropism and circadian rhythms (13, 31, 36, 53, 76). The focus of this section is on LOV domain proteins, namely the fungal Vivid (VVD) protein (16, 39). LOV domains utilize FMN or FAD as the chromophore for photosensing (40). The LOV domain family is a subset of the larger PAS domain family that functions in a variety of signaling pathways in prokaryotes and eukaryotes (72). Most members of the LOV protein family have multidomain structures that, in addition to the LOV domain, include serine/threonine kinase, histidine kinase, phosphodiesterase, Kelch repeats, and DNA binding domains (13). In multidomain LOV proteins such as phototropins, the LOV domain serves to modulate the activity of the functional domains or otherwise known as 'output' domains in response to light (15). The modular properties of LOV domains enables LOV proteins to be involved in a variety of light-mediated cell signaling pathways and biological processes (13, 15). Interested readers are encouraged to read more extensive reviews of the LOV family (13, 15).

VVD is a fungal protein from *Neurospora* that has been shown to regulate carotenoid biosynthesis and to have a role in modulating the circadian clock in response to blue light (64, 90). VVD is one of the smallest known LOV proteins (186 residues) as it lacks other functional or output domains (Fig. 2) (13). VVD acts as a negative regulator of light response and is required for certain physiological adaptations such as the down regulation of carotenoid biosynthesis in response to constant light exposure (90). VVD repression of light responses involves attenuation of the white collar complex (WCC) that is the main activator of light-regulated genes (9). WCC is comprised of white collar-1 (WC-1), the other main clock flavoprotein that also contains a LOV domain and white collar-2 (WC-2) (9). The mechanism by which VVD interferes with WCC is unclear as VVD lacks a nuclear localization signal and is thought to reside mainly in the cytosol (9, 27). In contrast, WC-1 is localized in the nucleus where along with WC-2 forms the WCC and binds to promoter regions of light responsive genes to activate transcription (9). Thus, the regulation of WCC and gene expression by VVD is thought to involve other effector protein partners which will need to be identified to understand how VVD participates in light sensing signal transduction pathways in *Neurospora* (9).

Recent work by Crane's group has captured X-ray crystal structures of VVD in the dark (oxidized) and light (reduced) states (90). These structures have provided exceptional insights into the mechanism of signal transduction in VVD and other related LOV domain blue-light sensors. For these

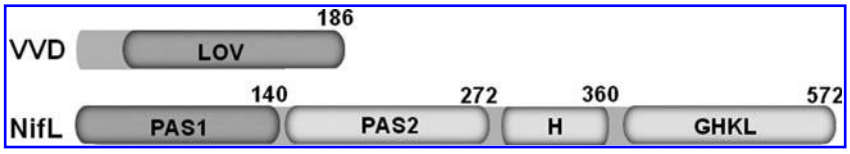

FIG. 2. Schematic outline of the domain structures of VVD and NifL. GHKL, gyrase; H, Histidine kinase like domain or motif; Hsp90, histidine kinase, MutL domain; LOV, light, oxygen or voltage domain; PAS1, FAD binding; PAS2, non-FAD binding.

structural studies, a truncated form of VVD that lacked N-terminal residues 1–36 was used. The structures of both the dark state and light state forms of VVD show it has a typical PAS domain α/β topology with the isoalloxazine ring of the FAD bound between two helices and three strands of the core β sheet (Fig. 3A) (90). In the dark state structure of VVD (2 Å resolution), residues 37–70 were observed to form a N-terminal α-helix (helix Aα) and were part of a structure referred to as the N-terminal cap (Fig. 3A). This N-terminal cap contacts the PAS β-sheet core and is thought to mediate VVD interactions with protein targets in response to light-induced signaling. Closer to the flavin, Cys108 was observed to be positioned above the C(4a) atom on the *si* face of the FAD which is a conserved residue in LOV domain proteins (90). Spectroscopic data have shown that upon excitation of the flavin with blue light, a cysteinyl-4a adduct is formed in LOV domain proteins with a peak at 390 nm (13, 31). The mechanism for the adduct formation involves light-initiated deprotonation of the cysteine thiol, followed by attack of the cysteine thiolate on the C(4a) atom of the flavin ring (31, 91). The result is that a covalently modified reduced flavin is formed in the light state (see Fig. 3B). Interestingly, the stability of the cysteinyl-4a adduct varies among LOV domain proteins with lifetimes ranging from 81 s (*Avena sativa* LOV2) to 5 h (VVD) (91). An extensive mechanistic study of VVD concluded that the rate limiting step in reversing the cysteinyl-4a adduct is deprotonation of the FAD N(5) atom (91).

The global conformational change induced by light reduction of the flavin is a substantial increase in the hydrodynamic volume of VVD that is primarily caused by increased disorder of the N-terminal region (90). Flavin redox signals that are emitted from the PAS domain induce conformational changes at the N-terminal that are proposed to regulate the monomer–dimer equilibrium of VVD and interactions with other proteins (89, 90). A new study using time-resolved small-angle X-ray scattering revealed that dissociation of the N-terminus from the PAS core is an important step in the light-induced conversion of VVD to the dimeric form (33). Figure 3B shows an alignment of the dark and light state structures of VVD that reveals exquisite details of a hydrogen bond pathway for communicating redox signals out of the FAD active site to the N-terminal region (90). The first notable difference between the dark and light state structures is the orientation of Gln182 near the flavin. In the dark state, the amide nitrogen of Gln182 forms a hydrogen bond with the FAD N(5) atom (90). In the light state, the Gln182 side chain is flipped relative to the dark state structure so that the Gln182 carbonyl is within hydrogen bonding distance of N(5)H (Fig. 3B) (90). The second interaction that is impacted by movement of Gln182 is with the backbone carbonyl of Ala72. Ala72 is part of a hinge region (residues 68–72) that links the N-terminal cap to the Aβ strand of the PAS core. In the dark state, the carbonyls of Ala72 and Gln182 appear to have an unfavorable contact (90). With the new orientation of Gln182 in the light state, however, a favorable hydrogen bond interaction is generated between the Gln182 amide and the backbone carbonyl of Ala72 (90). Thus, in the structure with the covalently reduced flavin (*i.e.*, light state) Gln182 mediates a hydrogen bond pathway from the FAD N(5)H to Ala72. Additionally, Cys71 forms a new hydrogen bond with the backbone amide of Asp68 in the light state (Fig. 3B) (90).

The net effect of the reorganized hydrogen bonding involving Gln182 and Cys71 is a closer positioning of the N-terminal cap residues to the core PAS domain. This movement toward the PAS core is proposed to alter the packing of helix Aα on the surface and lead to the release of a N-terminal peptide from VVD in the light state. The release of the N-terminal peptide region in response to light primarily leads to dimerization of VVD that may then allow VVD to engage with target proteins or compete with the WC-1LOV domain

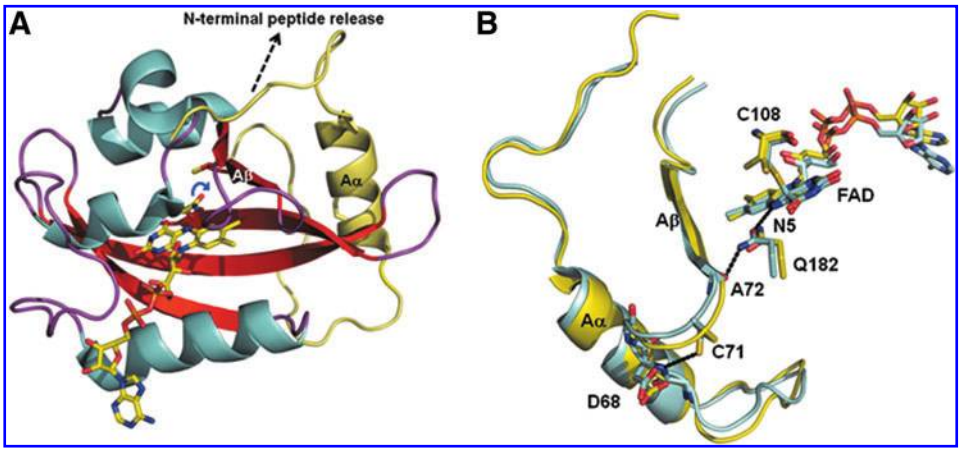

FIG. 3. The crystal structure of VVD. (A) Ribbon diagram of the VVD structure in the dark state (oxidized) with bound FAD cofactor (*yellow*). The N-terminal cap is highlighted in *yellow.* The Gln182 side chain is shown in the active site with the *blue arrow* showing that upon light exposure Gln182 flips to make a hydrogen bond with Ala72 near the Aβ strand. The *dashed arrow* (*black*) indicates the proposed release of the N-terminal region from VVD based on hydrodynamic studies of the light and dark states. **(B)** Superposition of VVD structures in the dark-oxidized state (*yellow*) and light-reduced state (*teal*). Shown for both structures are the FAD cofactors, Aβ strands and Aα helices, and residues Cys108, Gln182, Ala72, Cys71, and Aps68. The covalent adduct between C108 and the FAD C(4a) is only observed in the light state structure. Bridging hydrogen bonds are shown for Gln182 with the backbone carbonyl of Ala72 and the FAD N(H)5 in the light state structure of VVD. Also shown for the light state structure is the hydrogen bond between Cys71 and Asp68. The hydrogen bond network in the light state structure of VVD highlights the redox signal transduction pathway from the FAD N5 to N-terminal domain. Structural models were generated using PyMol and PDBs 2PD7 (dark state, oxidized) and 2PDR (light state, reduced). (For interpretation of the references to color in this figure legend, the reader is referred to the web version of this article at www.liebertonline.com/ars).

(89, 90). Consistent with Gln182 having a critical role in signal transmission, a Gln182Leu VVD mutant was shown to be defective in conformational switching in response to light (90). It should be noted that Gln182 is a highly conserved residue in the LOV domain family (91). Thus, the hydrogen bond pathway revealed for photoswitching in VVD is most likely a shared feature in other LOV domain proteins.

Recent high resolution structures of the LOV domain protein, YtvA, have provided additional insights into how light-induced changes in hydrogen bonding lead to structural rearrangements. YtvA is a photosensor from *Bacillus subtilis* that is involved in the general stress response pathway (4). In YtvA, a STAS (sulfate transporter and anti-sigma factor) effector domain is connected to the C-terminal end of the LOV domain via a linker α-helix. Structures of the dimeric LOV domain of YtvA in the dark and light states indicate that the α-helix linker moves away from the dimer interface in response to light (48). The structures also reveal a unique 5° rotation of the two monomers relative to each other (48). The light-induced rotation is thought to be propagated through the α-helix linker that extends out from the C-terminal end of the LOV domain (48). How this rotation regulates the GTP binding activity of the STAS domain remains to be elucidated. The structures of both VVD and YtvA provide evidence that signal transmission to either an N-terminal (*e.g.*, VVD) or C-terminal (*e.g.*, YtvA) α-helix on the surface of the LOV core is a key part of the light-induced structural changes that impact LOV domain interactions with effector modules.

NifL (Transcriptional Regulator of Nitrogen Fixation)

In diazotrophs such as *Azotobacter vinelandii*, the flavoprotein NifL represses the expression of the nitrogen fixation (*nif*) genes by forming an inhibitory complex with NifA, the σ^{54} dependent transcriptional activator of the *nif* genes (28, 43). The regulation of NifL–NifA interactions is multifaceted and involves responses to redox conditions and nitrogen status (43, 44). This review will focus on the redox regulation of the NifL–NifA complex (Fig. 4A). In response to oxidative

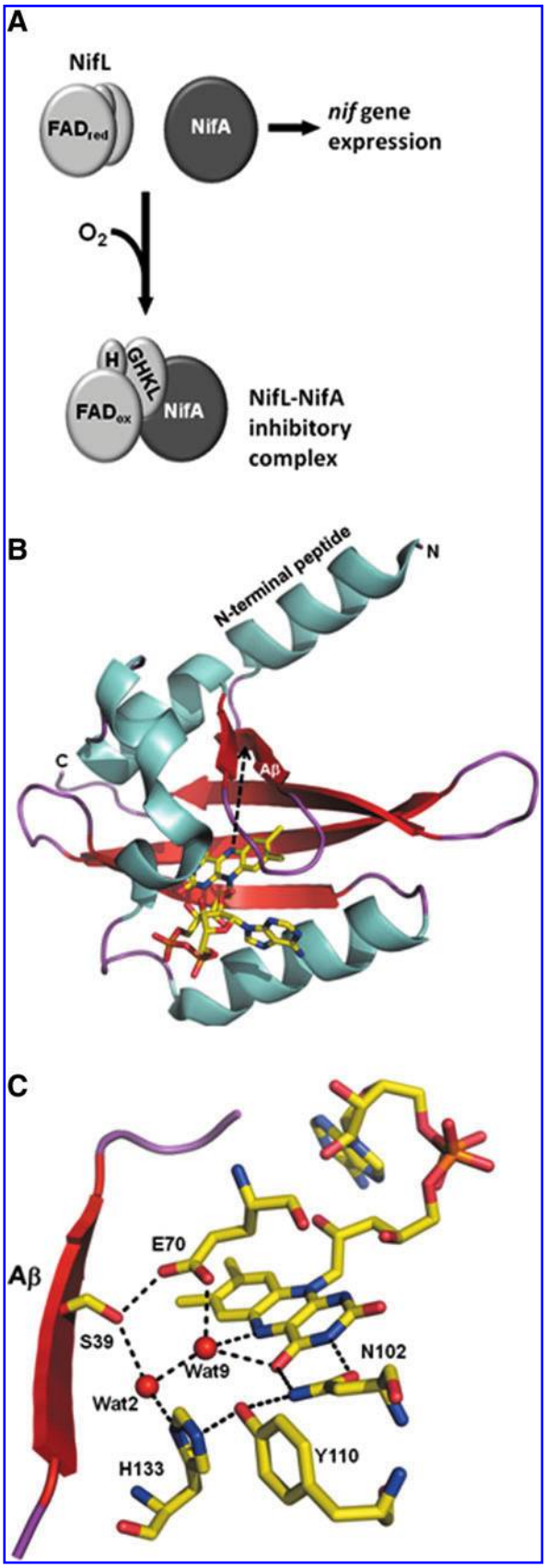

FIG. 4. Redox regulation of NifL. (A) Cartoon showing the general model for how NifL regulates NifA. Under reducing conditions in which the FAD cofactor is reduced, NifL does not form a stable complex with NifA, allowing nif gene expression to be activated by NifA. When oxygen levels rise, the reduced FAD cofactor reacts quickly with molecular oxygen to generate oxidized FAD, resulting in a conformational change that exposes the H- and GHKL-domains. These domains provide a surface for binding NifA, resulting in the formation of a NifL–NifA inhibitory complex that blocks activation of the nif genes. **(B)** Ribbon diagram of the PAS1 FAD binding domain from NifL in the oxidized state. The FAD cofactor is shown in *yellow*. The A*β* strand and the N-terminal peptide are labeled with a *black dashed arrow*, indicating the potential direction of a redox signal from the FAD N(5) position. **(C)** The active site of the PAS1 domain from NifL. Shown are the FAD cofactor and the hydrogen bond network linking the FAD N(5) atom to Ser39 of the A*β* strand. Structural diagrams were made with PyMol and PDB 2GJ3 for the PAS1 domain structure of NifL. (For interpretation of the references to color in this figure legend, the reader is referred to the web version of this article at www.liebertonline.com/ars).

intracellular conditions, NifL prevents unwanted production of nitrogenase (molybdenum dependent) during periods of aerobiosis by binding to NifA, thus acting as an anti-activator protein (28, 43). Under reducing conditions, NifL does not form a complex with NifA, thereby allowing NifA to activate the *nif* genes (28, 43). NifL contains a FAD-binding PAS domain that mediates the redox functional switching of NifL–NifA interactions (65, 66). Unlike VVD, NifL is a multidomain protein (519 residues) that contains two tandem PAS domains at the N-terminus (residues 1–252) with one PAS domain containing FAD (PAS1) and the second PAS domain (PAS2) devoid of any cofactor (PAS2) (see Fig. 2) (65). The C-terminal domain (residues 360–519) of NifL is homologous to the GHKL (gyrase, Hsp90, histidine kinase, MutL) superfamily while the middle region of NifL (253–359) shares homology with histidine kinase proteins that contain a HisKA domain (H-domain) (65). Despite these similarities, the H (HisKA) and C-terminal (GHKL) domains together do not exhibit histidine kinase activity but do function to provide the interface for binding to NifA (38, 65).

The physiological oxidant of NifL is molecular oxygen that rapidly reacts with the reduced FAD cofactor in PAS1 to produce H_2O_2 (29). This allows NifL to respond quickly to aerobic conditions and inhibit NifA. The physiological reductant for NifL, however, is not clear. The reduction potential for NifL (-196 mV, pH 7) is accessible to a number of potential electron donors (41). In *Klebsiella pneumoniae*, the respiratory quinone pool is thought to be a source of electron donors for NifL (23, 73). In order for NifL to be reduced by the quinone pool, NifL is proposed to shuttle between the membrane and the cytoplasm in *K. pneumoniae* (73). In considering the mechanism of redox switching in NifL, the focus has been more on conformational changes that occur during the transition from the reduced (noninhibitory) to the oxidized (inhibitory) state. The general model for NifL redox switching is that oxidation of the bound FAD cofactor in the PAS1 domain induces a conformational change that is propagated out to the H-domain and C-terminal domains (65). Structural changes in the H- and C-terminal domains then cause increased NifL–NifA binding affinity leading to inhibition of NifA (Fig. 4A) (38). The importance of the H-domain and PAS2 domain in the redox functional switching of NifL were recently shown by Dixon *et al.* (38, 65). First, mutating Arg306 in the H-domain generated a NifL mutant that constitutively bound NifA and was unresponsive to changes in the FAD redox state (38). Second, they were able to generate mutants in the PAS2 domain that locked NifL into a conformational state that makes it a constitutive inhibitor of NifA (65). They also engineered mutants in the PAS2 domain that locked NifL into a noninhibitory conformation that could not form a stable complex with NifA. Thus, the redox functional switching of NifL can be abolished by mutating certain residues in either the PAS2 or H-domains. These results indicate that the PAS2 and H-domains have a critical role in transducing redox signals from the PAS1 FAD domain and regulating NifL–NifA interactions.

Structural details into how redox signals are transmitted out from the FAD cofactor in NifL were recently gained from a 1.04 Å structure of the PAS1 domain (residues 1–140) solved by Moffat's group (29). The PAS1 domain of NifL is characterized by the usual α/β fold of PAS domains (Fig. 4B) (29). Because NifL reacts readily with molecular oxygen, it was of interest to determine potential access channels to the FAD. Multiple solvent access channels were found with two water molecules near the flavin, suggesting a feasible pathway for molecular oxygen to enter the active site and react with the C(4a) position of the reduced flavin and form a hydroperoxy intermediate (29). Also, a Glu residue (Glu70) was positioned on the *si* face of the isoalloxazine ring (Fig. 4C). The position of Glu70 is similar to that observed for Cys108 in the VVD structure. Glu70 makes hydrogen bond contacts with an active site water molecule and a nearby Ser39 residue (29). Glu 70 is suitably positioned to accept a proton from the FAD N(5) and may also interact with the hydroperoxy intermediate (29). Besides helping with the hydrolysis of the hydroperoxy intermediate, the water molecules contribute to a hydrogen bond network that links the N(5) and C(4)O atoms of the flavin with residues Ser39, Glu70, Asn102, Tyr110, and His133 (Fig. 4C) (29). This hydrogen bond network is proposed to be critical for redox sensing in NifL by facilitating protonation/deprotonation of the FAD N(5) (29). Based on these structural observations, it was proposed that redox signals from the flavin are transmitted to the surface of the PAS1 domain via Ser39 which resides on strand Aβ (Figs. 4B and 4C). The redox signals then generate an altered structure on the surface that perhaps involves changes in a N-terminal peptide as observed for VVD (Fig. 4 B) (29). These changes are then transmitted further to the H- and C-terminal (GHKL) domains to influence NifL–NifA binding affinity. Most likely, changes in the quaternary arrangement of the PAS2 domains occur that transmit redox signals from the PAS1 flavin domain to the C-terminal domains of NifL (65). It should be noted that the regulation of NifL–NifA interactions does not involve changes in oligomerization as NifL is a tetramer in both the oxidized and reduced states (29).

Pyruvate Oxidase (Enzyme Activated by Membrane Binding)

Pyruvate oxidase (POX) from *Escherichia coli* (*Ec*POX) is by far the most studied of the POX enzymes (1, 11, 22, 42, 50, 57–59, 61–63, 77, 79). *Ec*POX contains FAD and thiamin pyrophosphate (TPP) and catalyzes the oxidative decarboxylation of pyruvate to acetate and CO_2 (58, 59). POX has a homotetrameric structure consisting of 62 kDa subunits (572 residues), and when reduced, POX switches from a soluble cytosolic protein to a peripheral membrane-bound ubiquinone oxidoreductase (22, 42, 63, 77). The physiological role of POX in *E. coli* is to serve as an alternate system to the well known TCA cycle enzyme, the pyruvate dehydrogenase complex (PDHC) (1, 22). Expression of the POX encoding gene, *poxB*, is regulated by the sigma factor RpoS that induces the transcription of *poxB* in the early stages of the *E. coli* stationary growth phase (11). Thus, *Ec*POX is mostly expressed during times of slow growth when microaerobic conditions are prevalent (1, 11). Although PoxB-null strains showed that POX provides a significant contribution to aerobic growth efficiency, POX does not fully complement PDHC mutant strains as determined by growth rate, growth yields, and carbon conversion efficiencies as POX strains showed an approximate 20% decrease in growth efficiency compared to PDHC expressing strains (1).

Members of the POX enzyme superfamily are distinguished by well-defined catalytic and structural differences

even among prokaryotic enzymes (62). For example, POX enzymes can be divided according to the natural electron acceptor employed in the POX reaction cycle (62). Even though *Ec*POX is called a pyruvate "oxidase", it is well established that the physiological electron acceptor is membrane-bound ubiquinone-8 (10, 30, 42). Therefore, this enzyme has been more accurately referred to as a pyruvate:quinone oxidoreductase (PQO) (62). In contrast, other prokaryotic POX enzymes readily use O_2 as the electron acceptor and are thus true oxidases generating H_2O_2 during every catalytic cycle (62). One well-studied example is POX from *Lactobacillus plantarum* (*Lp*POX) (49, 79). *Lp*POX not only differs from *Ec*POX in oxygen reactivity, but also uses P_i to produce acetylphosphate (49). Very little is known about how these aforementioned differences relate to the physiological and regulatory functions of POX enzymes (62). According to a recent phylogenetic survey of PQO type (*e.g.*, *Ec*POX) and POX type (*e.g.*, *Lp*POX) enzymes, it appears that they are interspersed in gram positive and gram negative bacteria lineages (62). In the same study, physiological experiments with *Corynebacterium glutamicum*, a gram-positive aerobe expressing a PQO type enzyme, suggested that this enzyme is regulated by carbon sources rather than growth phase as observed for *Ec*POX (61, 62). The authors concluded that the difference in the surrounding genetic makeup of the *C. glutamicum pqo* gene compared to the *poxB* gene in *E. coli* were most likely responsible for the regulational differences (61, 62). With a paucity of literature on PQO type enzymes from organisms other than *E. coli*, the remainder of this section will focus on *Ec*POX.

As mentioned above, *Ec*POX is a TPP-containing flavoprotein that switches from a cytosolic protein to a membrane bound protein upon reduction of its flavin cofactor in order to reduce ubiquinone in the inner membrane (58, 59). The fact that the reduced form of *Ec*POX binds the membrane and is subsequently activated has been known for many years, but a detailed mechanism has yet to be identified (63). Early studies showed that when *Ec*POX was incubated with pyruvate, TPP, Mg^{2+}, and lipids or detergents, that the enzyme not only associated with lipids but its turnover number increased 25-fold and the K_m for pyruvate decreased by about 10-fold (14, 46, 59). A similar increase in activity was observed by limited proteolysis of *Ec*POX with α-chymotrypsin under reducing conditions, suggesting a conformational change in the enzyme was responsible for the dramatic increase in activity (57–59). The trigger for this apparent conformational change was shown to be reduction of the FAD cofactor by pyruvate (59). Interestingly, partially digested *Ec*POX was unable to associate with lipids or detergents, indicating a membrane-binding domain was removed during limited proteolysis (59). Limited proteolysis of the reduced enzyme produces a 2.6-kDa peptide referred to as the α-peptide that independently associates with phospholipids, suggesting that this peptide was the membrane-binding domain (56, 82). The same conclusion was reached from *in vivo* work using an *Ec*POX construct with a truncated C-terminus to mimic the proteolytically cleaved enzyme (21). Site-directed mutagenesis of the C-terminus also confirmed the peptide region was critical for *Ec*POX lipid binding (20). After a decade of work firmly establishing the C-terminus as the membrane-binding domain of *Ec*POX, the reversibility of *Ec*POX membrane binding was later shown using surface plasmon resonance (SPR) (*42*). Furthermore, an electrochemical approach was used to monitor the kinetics of ubiquinone reduction in a model lipid bilayer, showing that membrane binding and ubiquinone reduction kinetics shared a similar profile (*42*). This demonstrated that only the membrane-bound enzyme could turnover with the lipid bound quinone pool (*42*).

Recently, structures of full-length *Ec*POX (1–572) and a truncated form of *Ec*POX (1–549) that lacks the 23-residue C-terminal peptide were solved (50). These structures have shed atomic details (3 to 2.5 Å respectively) on the long-standing putative membrane-binding domain as well as on a possible mechanism for how flavin reduction activates *Ec*POX membrane binding and leads to catalytic enhancement (50). The full-length structure of *Ec*POX corresponds to the less active cytosolic form, while the structure of truncated *Ec*POX most likely represents the activated membrane-bound form. Figure 5A shows the monomeric structure of full-length *Ec*POX. A major difference between the full-length and truncated protein is the substantial increase in solvent exposure of the flavin cofactor in the cleaved form of the enzyme compared to the full-length enzyme (50). The increased solvent exposure, as also suggested by the UV-visible flavin spectrum of truncated *Ec*POX, may explain the 10-fold decrease in the K_m for pyruvate with the activated form of the enzyme (50, 57). The structures of the full-length and truncated forms of *Ec*POX also provide a mechanistic rationale for the 20–30-fold increase in activity seen with the activated form of *Ec*POX (50). A key structural difference found between the full-length and C-terminal truncated forms of *Ec*POX involves active site residue Phe465 (50). In a structural alignment between full-length *Ec*POX and *Lp*POX, it was recognized that Phe465 from *Ec*POX and the corresponding Phe479 residue in *Lp*POX were oriented differently in reference to the flavin cofactor (50). In *Lp*POX, Phe479 is turned more toward the isoalloxazine ring of the flavin compared to *Ec*POX Phe465 (50). In the C-terminal truncated form of *Ec*POX, Phe465 is positioned similarly to Phe479 in *Lp*POX with respect to the flavin ring (50). Figure 5B shows an overlay of the full-length and truncated *Ec*POX forms highlighting the different orientations of Phe465. Intriguingly, *Lp*POX is known to be constitutively active with inter-cofactor electron transfer rates mimicking the lipid-activated form of *Ec*POX ($400\ s^{-1}$) (6, 74). Thus, although TPP and FAD are only 7 Å apart, the inter-cofactor positioning of Phe465 in the C-terminal truncated form of *Ec*POX appears to make electron transfer more efficient between TPP and FAD (50). Therefore, the alignment provides structural reasoning to support the higher catalytic activity of *Lp*POX and the C-terminal truncated form of Ec-POX relative to full-length *Ec*POX (50).

To summarize the activation mechanism of *Ec*POX, the TPP cofactor of *Ec*POX is first reduced by pyruvate with subsequent electron transfer to the FAD cofactor. Reduction of the flavin cofactor then triggers the release of the C-terminal membrane binding domain, thereby opening up the active site which allows for Phe465 to swing into a position that facilities electron transfer from TPP to FAD in subsequent catalytic cycles. This activated conformation of Phe465 in *Ec*POX is thought to mimic Phe479 in *Lp*POX, explaining similar turnover numbers between the activated form of *Ec*-POX and the constitutively active *Lp*POX.

The new orientation of Phe465 in the C-terminal truncated form of *Ec*POX is also proposed to have a role in regulating

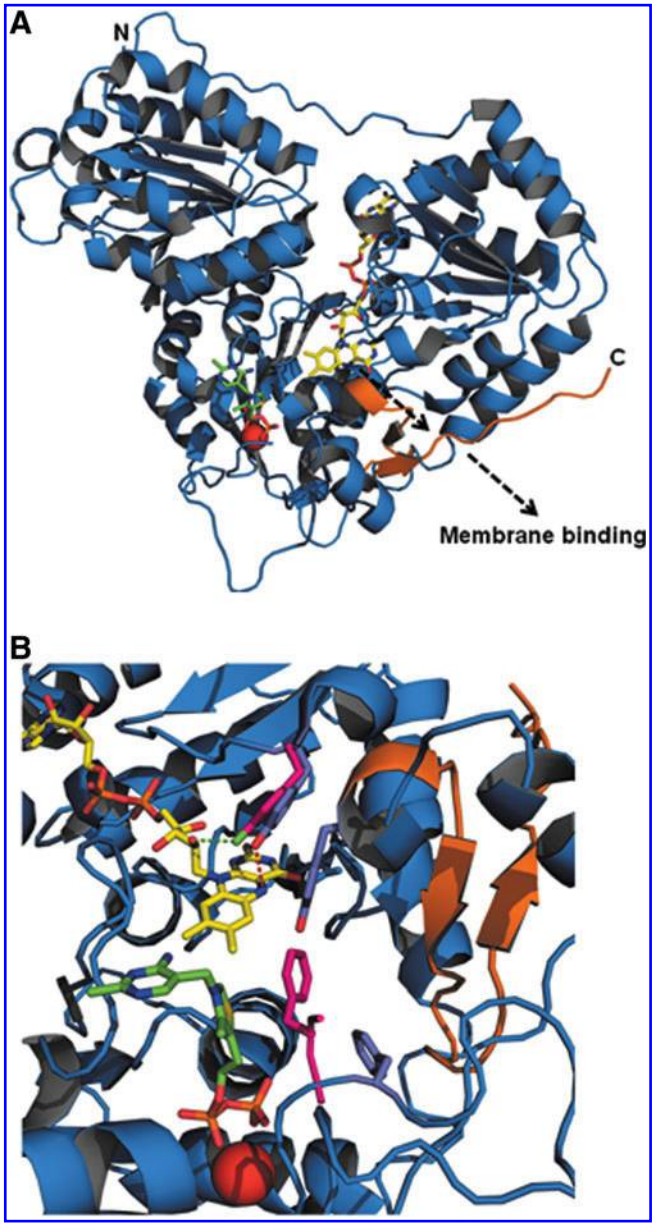

FIG. 5. EcPOX structure and alignment. (A) Full-length structure of EcPOX monomer shown in cartoon, with TPP and FAD shown as *sticks*, and Mg^{2+} shown as a *red sphere*. FAD and TPP are colored *yellow* and *green*, respectively. The residues that make up the C-terminal peptide (550–572) are colored *orange*. The N and C-terminus are labeled N and C, respectively. The *dashed black arrow* indicates the release of the C-terminal peptide from the surface triggered by FAD reduction. **(B)** Overlay of the full-length (1–572) and C-terminal truncated (1–549) structures of EcPOX. Coloring is the same as in **(A)**. The side chains for Y278 and F465 are shown in the overlay as *sticks* and colored in *light purple* and *bright pink* for the full-length and truncated structures, respectively. The side chain for Y549 is also shown but is only seen in the full-length structure. The structures were modeled using PyMol and PDB accession codes 3EY9 (full-length structure) and 3EYA (truncated structure). (For interpretation of the references to color in this figure legend, the reader is referred to the web version of this article at www.liebertonline.com/ars).

*Ec*POX membrane binding (50). In the full-length structure of *Ec*POX, Tyr549 would interfere with the new position of Phe465 based on an overlay of the full-length and truncated *Ec*POX structures (Fig. 5B) (50). Thus, Tyr549 would need to be displaced to avoid a steric clash with Phe465. This displacement of Tyr549 apparently occurs in truncated *Ec*POX since the electron density in this region of the protein is not well defined (50). Because Tyr549 is adjacent to the membrane binding C-terminal peptide (residues 550–572), it was suggested that movement of Phe465 toward the flavin would cause displacement of Tyr549 and subsequent release of the C-terminal peptide (50). Another Tyr that could also have an important role in transmitting redox signals is Tyr278 which forms hydrogen bonds to both the N(5) atom and the ribityl 2′-OH group (Fig. 5B).

Lastly, structural details concerning conformational transitions that occur in the C-terminal peptide upon release from *Ec*POX and membrane binding should be noted. In the full-length structure of *Ec*POX (1–572 residues), the C-terminal end (last 23 amino acids, residues 550–572) is secured to the flavin active site domain by a number of electrostatic and hydrogen bonding partners (50). Also, residues 550–564 form a two-stranded antiparallel β-sheet. A synthetic C-terminal peptide molecule was studied independently of *Ec*POX by circular dichroism to define possible structural changes that occur upon release from *Ec*POX and membrane binding. In the absence of detergent, the peptide was found to adopt a random secondary structure. In the presence of detergent, the peptide molecule adopted an α-helix structure (50). The data predicts that upon releasing from *Ec*POX, the C-terminal peptide initially transitions into a partially random structure and then into an amphipathic α-helix once it binds the membrane (50).

PutA Protein (Transcriptional Regulator and Membrane-Bound Enzyme)

Proline utilization A (PutA) from *E. coli* (*Ec*PutA) is a flavoprotein that functions as a transcriptional repressor and a membrane-bound proline catabolic enzyme. Figure 6A shows the enzymatic functions of *Ec*PutA which are two-fold, involving a proline dehydrogenase (PRODH) domain that catalyzes the flavin-dependent oxidation of proline to Δ^1-pyrroline-5-carboxylate (P5C) and a P5C dehydrogenase (P5CDH) domain that catalyzes the NAD^+-dependent conversion of γ-glutamic acid semialdehyde (GSA) to glutamate (2, 47, 60). GSA is formed by the hydrolysis of P5C, a reaction which is presumably nonenzymatic. The dual enzymatic activities of *Ec*PutA are shared among PutA proteins in gram-negative bacteria and are referred to as bifunctional PutAs (71). In certain gram-negative bacteria such as *E. coli* and *Salmonella typhimurium*, PutA proteins also have a N-terminal DNA binding domain that endows them with transcriptional regulatory activity (71). In these bacteria, PutA represses expression of the *putA* and *putP* (high-affinity Na^+-proline transporter) genes under low proline conditions (85). PutA repression of the *put* genes is relieved by increases in proline levels with maximum *put* gene expression occurring under poor nutrient conditions (85). Thus, PutAs with DNA binding activity are trifunctional flavoproteins that act as sensors of cellular metabolism by responding to fluctuations in proline levels (Fig. 6B).

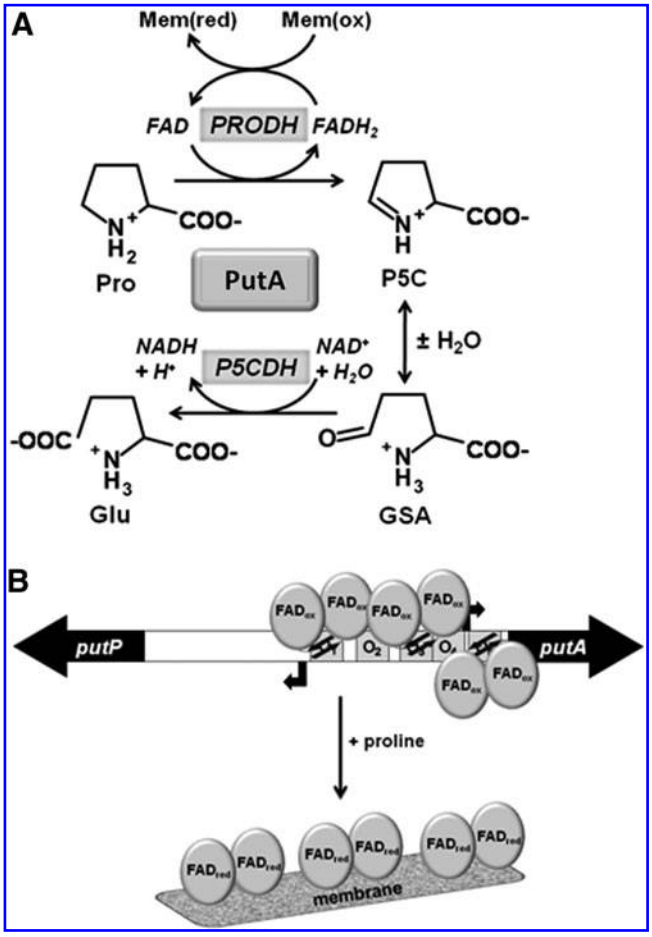

FIG. 6. Multiple functions and regulation of PutA. (A) Reactions catalyzed by PutA. **(B)** Overall model of PutA functional switching. In the absence of proline, the flavin cofactor is oxidized and PutA accumulates on the DNA, repressing expression of the put genes. The five PutA binding sites are labeled as O1, O2, O3, O4, and O5. The *black arrows* represent the β-strands of the RHH domain that binds the DNA. When proline is available, the flavin cofactor is reduced by PutA, resulting in activation of PutA-membrane binding. The change in intracellular location of PutA in response to proline relieves repression of the *put* regulon.

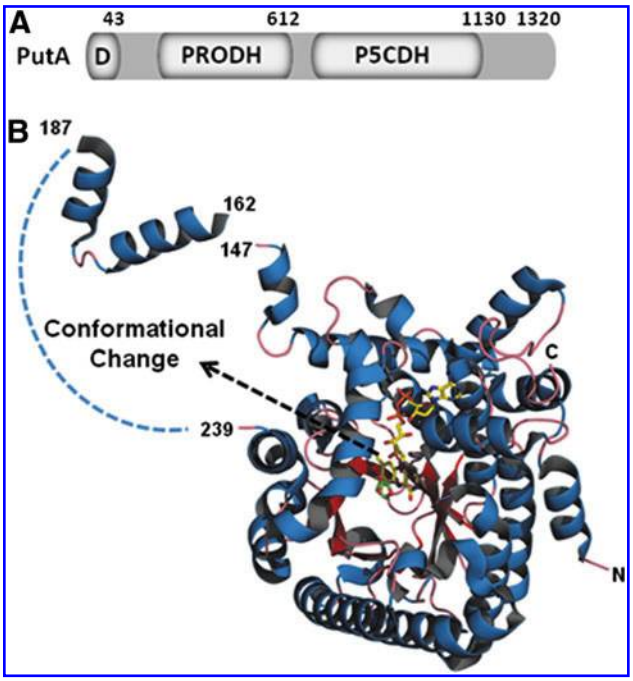

FIG. 7. Structural architecture of PutA. (A) Domain map of PutA. **(B)** Structural model of the PRODH domain (residues 86–630) complexed with L-THFA. The model shows the β/α barrel structure with the bound FAD cofactor (*yellow*) and L-THFA (*green*) in the active site. The *dashed curve* represents residues that are not observed in the structure, including Trp211 and Arg234. The *dashed arrow* indicates that redox signals from the flavin result in conformational changes in a disordered region outside the PRODH active site. The model was made using Pymol and PDB 1TIW. (For interpretation of the references to color in this figure legend, the reader is referred to the web version of this article at www.liebertonline.com/ars).

*Ec*PutA is a polypeptide of 1320 amino acids with the DNA-binding, PRODH, and P5CDH domains localized to residues 2–43, 261–612, and 650–1130, respectively (7, 37) (Fig. 7A). The DNA-binding domain of *Ec*PutA includes N-terminal residues 2–43 that form a dimer independently of the PutA polypeptide (24, 34). X-ray crystal and NMR structures of the N-terminal domain show it has a ribbon-helix-helix (RHH) structure, making PutA a member of the RHH superfamily of transcriptional regulators (25, 34). In RHH proteins, the β-sheet recognizes the major groove of the DNA. The PRODH domain forms a β/α-barrel active site which contains a non-covalently bound FAD cofactor (35) (Fig. 7B). The full-length structure of *Ec*PutA has not been solved but recently a full-length structure of a bifunctional PutA enzyme from *Bradyrhizobium japonicum* was solved by Tanner's group that shows how the PRODH and P5CDH domains are arranged (68). The structure provides evidence for substrate channeling of the intermediate P5C/GSA between the PRODH and P5CDH active sites that are separated by 40 Å (68).

In the absence of proline, *Ec*PutA resides in the cytoplasm and acts as a transcriptional repressor of the *put* genes (7, 52). PutA represses the *put* genes by binding to five operator sites in the 419 bp intergenic control region from which the *putP* and *putA* genes are transcribed in opposite directions (7, 51, 52, 85) (Fig. 6B). PutA recognizes a 5′-GTTGCA-3′ sequence motif that is conserved in each operator site (85). Binding of PutA to the operator sites most likely interferes with σ^{70}-dependent binding of *E. coli* RNA polymerase, thus blocking transcription of the *putA* and *putP* genes. In the presence of proline, PutA binds to the inner cytoplasmic membrane and functions as an enzyme where it catalyzes the oxidation of L-proline to glutamate (Fig. 6B) (8, 51, 84). Similar to *Ec*POX, *Ec*PutA association with the membrane is critical to complete the reaction cycle as the reduced FAD formed in the PRODH reductive half-reaction is converted back to oxidized FAD by electron transfer to ubiquinone in the cytoplasmic membrane (oxidative half-reaction) (Fig. 6A) (80).

The switching of *Ec*PutA between DNA-binding and enzymatic functions necessitates a change in intracellular location in response to proline. The ability of *Ec*PutA to directly respond to proline is dependent on the activity of the PRODH

domain and the flavin redox state. Studies were performed to determine whether changes in the flavin redox state impacted *Ec*PutA-DNA or *Ec*PutA-membrane binding affinities. Analysis of *Ec*PutA-DNA interactions by spectroelectrochemistry and SPR under conditions in which the bound flavin cofactor is reduced indicated no significant differences in *Ec*PutA DNA binding affinity relative to oxidized *Ec*PutA (5, 86). Thus, it was concluded that the intracellular location of *Ec*PutA is not caused by displacing *Ec*PutA from the DNA.

In contrast, the flavin redox state has been shown to have a profound influence on *Ec*PutA–membrane interactions. In earlier work, proline was shown to induce *Ec*PutA-membrane binding (8, 80). Western blot analysis has shown that proline shifts the intracellular location of *Ec*PutA from the cytosol to the membrane, consistent with membrane binding being critical for activation of *put* gene expression (86). SPR studies have provided kinetic details of this phenomenon showing that oxidized PutA does not bind to immobilized *E. coli* polar lipid vesicles. Upon reduction of the flavin with either proline or dithionite, however, a tight *Ec*PutA–membrane complex is formed, indicating that flavin reduction alone is sufficient to induce *Ec*PutA–lipid binding (83). Thus, the FAD redox state governs the intracellular location of *Ec*PutA, thereby enabling *Ec*PutA to undergo a switch from a transcriptional repressor to a membrane-bound enzyme in response to proline. Although *Ec*PutA membrane binding is necessary to relieve *Ec*PutA repression of the *put* genes, membrane localization of *Ec*PutA in general is not sufficient to activate *put* gene expression. When *Ec*PutA is fused to the membrane via LacY, it can still repress *put* gene expression (86). This is consistent with the model that protein–membrane localization does not generally prevent proteins from binding chromosomal DNA in bacteria (19). Thus, reduced *Ec*PutA must be specifically positioned on the membrane to prevent *Ec*PutA–DNA binding.

The flavin redox switch in *Ec*PutA-membrane complexes involves global conformational changes that significantly enhance *Ec*PutA-membrane binding. A relative increase in the overall hydrophobicity of *Ec*PutA by proline was proposed to lead to increased membrane binding (70). A proline-dependent conformational change was also identified by limited proteolysis studies that coincides with proline activation of *Ec*PutA–membrane binding (8). Controlled potentiometric proteolysis of *Ec*PutA demonstrated a reversible conformational change occurs near Arg234 with a redox potential that closely matches the reduction potential of the bound FAD (-77 mV, pH 7.5) (88). Intrinsic fluorescence studies of *Ec*PutA also identified conformational changes that occur near Trp211 (87). Residues Arg234 and Trp211 reside in a disordered region that is just outside the PRODH active site (Fig. 7B). Thus, both limited proteolysis and fluorescence studies identified a region near the PRODH domain that undergoes a conformational change in response to the redox state of the FAD cofactor. How this disordered region contributes to enhanced *Ec*PutA–membrane binding is not known but may directly involve membrane binding or interactions with another domain that is responsible for membrane binding.

Although the complete redox-dependent structural transition that occurs in the *Ec*PutA polypeptide is not fully understood, molecular details of signal transmission from the FAD cofactor are beginning to emerge. The initial structures of the *Ec*PutA PRODH domain were of the FAD in the oxidized state with competitive inhibitors such as L-tetrahydro-2-furoic acid (L-THFA) bound in the active site (35, 81). These structures revealed the importance of Arg555 and Arg556 in substrate binding as both residues form ion pairs with the carboxylate group of proline. In addition, Arg431 forms a hydrogen bond with the FAD N(5) atom (3.1 Å) (Fig. 8). Recently, however, Tanner's group has solved two structures of the *Ec*PutA PRODH domain in a reduced state which have provided new insights into conformational changes in the FAD and the surrounding residues relative to the THFA-bound oxidized structure. In the first reduced structure, the PRODH domain crystal form was reduced with dithionite (83). In the second structure, *N*-propargylglycine (PPG) was used to covalently modify the FAD (69). PPG irreversibly inactivates *Ec*PutA by generating a three carbon link between active site residue K329 and the FAD N(5) atom. *Ec*PutA inactivated by PPG displays lipid binding properties similar to proline-reduced *Ec*PutA (69). In addition, limited proteolysis of PPG-inactivated *Ec*PutA indicated that the inactivated enzyme is locked into a conformation that resembles proline-reduced *Ec*PutA. Thus, it was proposed that PPG inactivated *Ec*PutA mimics the proline-reduced, membrane-bound form of PutA (69).

Examination of both the dithionite-reduced and PPG-inactivated PRODH domain structures revealed a significant "butterfly" bend (22°-35°) of the isoalloxazine ring that was

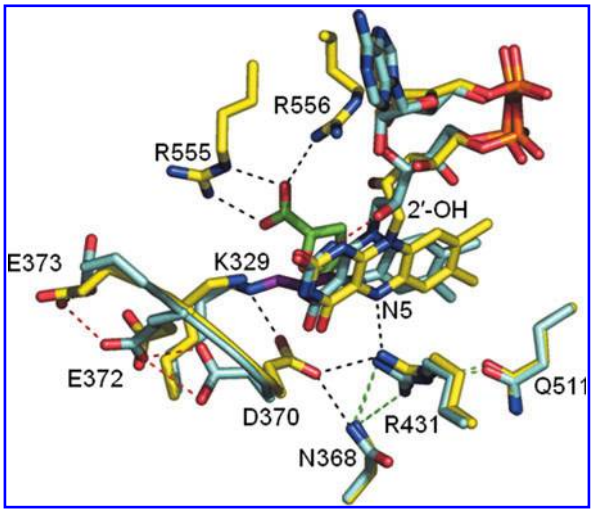

FIG. 8. Structural differences between THFA-bound and PPG inactivated PutA. THFA-bound (*yellow*) and PPG-inactivated (*teal*) PRODH structures were aligned. Shown are the bound FAD cofactors and key active site residues. THFA is shown in *green,* and the three-carbon link between Lys329 and the FAD N5 is shown in *purple* for the PPG-inactivated PRODH structure. Hydrogen bonds that are observed in both structures are in *green*. Unique hydrogen bond interactions in the THFA-bound structure are shown in *black*, and hydrogen bond interactions that are only observed in the PPG-inactivated structure are shown in *red*. Models were generated using PyMol and the PDB codes for THFA-bound (1TIW) and for the PPG-inactivate enzyme (3ITG). (For interpretation of the references to color in this figure legend, the reader is referred to the web version of this article at www.liebertonline.com/ars).

not observed in the L-THFA bound structure (69, 83). Another significant conformational change in the FAD cofactor was the formation of a new hydrogen bond between the 2′-OH ribityl group and the FAD N(1) position (69, 83). In crystal structures of oxidized PRODH, the 2′-OH ribityl group of FAD hydrogen bonds to Arg556, thus, reduction of the FAD causes the 2′-OH group to rotate 90° (83) (Fig. 8). Conformational changes were also observed for the ribityl 3′-OH and 4′-OH groups.

Further analysis of the PPG-inactivated structure revealed unique orientations of key active site residues relative to the THFA-bound structure (83). Figure 8 shows an alignment of the oxidized THFA-bound and PPG-inactivated structures. Conformational changes involving Arg431 and Asp370 were observed that potentially could be relevant to flavin signaling. The distance between Arg431 and the FAD N(5) is increased to 4.2 Å in the PPG inactivated structure from 3.1 Å observed in the THFA-bound form (69). Thus, the Arg431-N(5) interaction is disrupted in the PPG structure, suggesting a potential role for Arg431 in mediating redox signals. Another altered interaction in the PPG structure involves Asp370. In the THFA-bound structure, Asp370 hydrogen bonds to Arg431. In the PPG inactivated form, Asp370 is rotated away from Arg431 and forms a new hydrogen bond to Glu372 that forms a water-mediated hydrogen bond with Glu373 (Fig. 8) (69). Asp370, Glu372, and Glu373 are part of a β_3–α_3 loop that is on the surface of the PRODH domain. Based on these observations, Asp370, Arg431, and FAD N(5) were proposed to form an electrostatic network that communicates redox signals to a distal membrane binding domain on *Ec*PutA (69).

The roles of the 2′-OH group and Arg431 in the proline activation of *Ec*PutA-membrane binding was tested by site-directed mutagenesis and flavin analog studies. Disrupting the hydrogen bonding interactions of the 2′-OH group and Arg431 were shown to have severe consequences on PutA membrane binding. Removal of hydrogen bond interactions with the 2′-OH ribityl group by site-directed mutagenesis of Arg556 or replacement of normal FAD with 2′-deoxy-FAD significantly diminished the regulation of PutA-membrane binding (83). The 2′-OH ribityl group was therefore proposed to behave as a toggle switch between oxidized and reduced FAD to control the membrane binding affinity of PutA (83). Mutation of Arg431 to Met abolished the PutA–membrane binding under reducing conditions, showing that Arg431 has a critical role in the redox functional switching mechanism of PutA (83). Future studies are now needed to examine whether redox signals are further transmitted out of the flavin active site via the residue Asp370 and the nearby Glu residues of the β_3-α_3 loop.

Another important study will be to identify residues involved in membrane binding. Amino acid sequence alignment of various PutA family members reveals that trifunctional PutAs are generally longer polypeptides (1273–1320 residues) than bifunctional PutA proteins that lack DNA-binding activity such as PutA from *B. japonicum* (999 residues) (32). Besides the additional N-terminal residues encoding the RHH domain, trifunctional PutAs have 150–190 extra residues at the C-terminus relative to most bifunctional PutAs. This conserved C-terminal extension in trifunctional PutAs implies that the C-terminus may have an important functional role such as membrane binding (86).

Conclusion

The proteins highlighted in this review provide various mechanistic details of how flavin switches can govern protein function and intracellular location. By examining the architecture of these different flavin switch proteins, it is evident that hydrogen bond networks that link the flavin N(5) to the surface of the protein is a common theme. Hydrogen bond networks are important in flavin redox chemistry for mediating the uptake and release of protons in the active site, particularly at the flavin N(5). For flavin switch proteins, the internal hydrogen bond rearrangements and electrostatic networks are also critical for transmitting redox signals out of the flavin active site (29). The hydrogen bond pathway responsible for propagating redox signals to the surface of the protein is especially apparent for VVD, YtvA, and NifL, which share a PAS domain fold. Previously, it was proposed that PAS domain proteins share a common mechanism for transmitting flavin redox signals (29). A similar hydrogen bond network has also been observed for the BLUF domain protein, AppA, which is a FAD sensor protein from *Rhodobacter sphaeroides* involved in regulating photosynthesis genes (3, 40). Important hydrogen bonding residues are also evident in the active sites of *Ec*POX and *Ec*PutA. In *Ec*PutA, a pair of Glu residues appears to be optimally positioned to relay signals from the FAD N(5) to the protein surface, while *Ec*POX has a Tyr residue (Tyr278) that bridges the FAD N(5) and the ribityl 2′-OH group. Interestingly, the FAD ribityl 2′-OH group in *Ec*PutA has been proposed to act as redox toggle switch for controlling *Ec*PutA-membrane binding. The redox regulation of *Ec*POX may also feature a steric clash between two active site residues (Phe465 and Y549) that contributes to the signal transduction pathway and results in release of the C-terminal membrane binding peptide. For VVD, YtvA, NifL, and *Ec*POX, redox input signals induce a structural change that causes release of a peptide region that subsequently engages other proteins or in the case of *Ec*POX binds to the membrane. The redox-induced structural changes that occur on the surface of *Ec*PutA are not yet known but most likely involve exposure of a membrane binding domain.

Other proteins that undergo a flavin redox switch will continue to appear. The PAS domain family provides numerous examples of flavin-based sensors and provides the opportunity to explore how the PAS flavin binding domain can be used in diverse signaling pathways. A well-known example is the membrane-localized Aer PAS domain protein which utilizes a flavin to sense oxygen gradients (55, 78). Another example is *Ax*DGC2 (DGC2 protein from *Acetobacter xylinum*) that synthesizes the signaling molecule cyclic di-GMP (54). *Ax*DGC2 contains a PAS flavin domain and two catalytic domains with diguanylate cyclase (GGDF domain) and cyclic di-GMP phosphodiesterase (EAL domain) activities (54). Oxidation of the FAD in the PAS domain increases the activity of the GGDF domain, leading to higher cyclic di-GMP levels and increased cellulose synthesis in response to oxygen (54). Recently, the structure of a multidomain PAS protein (MmoS) from *Methylococcus capsulatus* was reported (75). MmoS regulates the expression of soluble methane monooxygenase depending on the levels of copper in the cell. It will be interesting to see how this PAS FAD domain senses copper and propagates the signal to other effector domains. Other flavoproteins unrelated to the PAS family are also potential

flavin redox switch proteins. These include the quinone reductase in yeast that is associated with the 20S proteosome and recruits Yap4, and the apoptotic-inducing factor that mediates protein–protein interactions and changes intracellular location (12, 67). Unraveling the mechanistic details of how flavin redox signals are converted into novel functional outputs will continue to be a fascinating area of research.

Acknowledgments

We thank former members of the laboratory group and Dr. John J. Tanner for providing insightful discussions about the *Ec*PutA structures. The work described for *Ec*PutA was supported in part by National Institutes of Health Grants GM061068 and P20 RR-017675.

References

1. Abdel–Hamid AM, Attwood MM, and Guest JR. Pyruvate oxidase contributes to the aerobic growth efficiency of *Escherichia coli*. *Microbiology* 147: 1483–1498, 2001.
2. Abrahamson JLA, Baker LG, Stephenson JT, and Wood JM. Proline dehydrogenase from *Escherichia* K12, properties of the membrane-associated enzyme. *Eur J Biochem* 134: 77–82, 1983.
3. Anderson S, Dragnea V, Masuda S, Ybe J, Moffat K, and Bauer C. Structure of a novel photoreceptor, the BLUF domain of AppA from *Rhodobacter sphaeroides*. *Biochemistry* 44: 7998–8005, 2005.
4. Avila- Perez M, Vreede J, Tang YF, Bende O, Losi A, Gartner W, and Hellingwerf K. *In vivo* mutational analysis of YtvA from *Bacillus subtilis.* Mechanism of light activation of the general stress response. *J Biol Chem* 284: 24958–24964, 2009.
5. Becker DF and Thomas EA. Redox properties of the PutA protein from *Escherichia coli* and the influence of the flavin redox state on PutA–DNA interactions. *Biochemistry* 40: 4714–4722, 2001.
6. Bertagnolli BL and Hager LP. Activation of *Escherichia coli* pyruvate oxidase enhances the oxidation of hydroxyethylthiamin pyrophosphate. *J Biol Chem* 266: 10168–10173, 1991.
7. Brown E and Wood JM. Redesigned purification yields a fully functional PutA protein dimer from *Escherichia coli*. *J Biol Chem* 267: 13086–13092, 1992.
8. Brown ED and Wood JM. Conformational change and membrane association of the PutA protein are coincident with reduction of its FAD cofactor by proline. *J Biol Chem* 268: 8972–8979, 1993.
9. Brunner M and Kaldi K. Interlocked feedback loops of the circadian clock of *Neurospora crassa*. *Mol Microbiol* 68: 255–262, 2008.
10. Carter K and Gennis RB. Reconstitution of the ubiquinone-dependent pyruvate oxidase system of *Escherichia coli* with the cytochrome o terminal oxidase complex. *J Biol Chem* 260: 10986–10990, 1985.
11. Chang YY, Wang AY, and Cronan JE, Jr. Expression of *Escherichia coli* pyruvate oxidase (PoxB) depends on the sigma factor encoded by the rpoS (katF) gene. *Mol Microbiol* 11: 1019–1028, 1994.
12. Churbanova IY and Sevrioukova IF. Redox-dependent changes in molecular properties of mitochondrial apoptosis-inducing factor. *J Biol Chem* 283: 5622–5631, 2008.
13. Crosson S, Rajagopal S, and Moffat K. The LOV domain family: Photoresponsive signaling modules coupled to diverse output domains. *Biochemistry* 42: 2–10, 2003.
14. Cunningham CC and Hager LP. Crystalline pyruvate oxidase from *Escherichia coli*. 3. Phospholipid as an allosteric effector for the enzyme. *J Biol Chem* 246: 1583–1589, 1971.
15. Demarsy E and Fankhauser C. Higher plants use LOV to perceive blue light. *Curr Opin Plant Biol* 12: 69–74, 2009.
16. Dunlap JC and Loros JJ. How fungi keep time: Circadian system in *Neurospora* and other fungi. *Curr Opin Microbiol* 9: 579–587, 2006.
17. Forneris F, Battaglioli E, Mattevi A, and Binda C. New roles of flavoproteins in molecular cell biology: Histone demethylase LSD1 and chromatin. *FEBS J* 276: 4304–4312, 2009.
18. Fraaije MW and Mattevi A. Flavoenzymes: Diverse catalysts with recurrent features. *Trends Biochem Sci* 25: 126–132, 2000.
19. Gorke B, Reinhardt J, and Rak B. Activity of Lac repressor anchored to the *Escherichia coli* inner membrane. *Nucleic Acids Res* 33: 2504–2511, 2005.
20. Grabau C, Chang YY, and Cronan JE, Jr. Lipid binding by *Escherichia coli* pyruvate oxidase is disrupted by small alterations of the carboxyl-terminal region. *J Biol Chem* 264: 12510–12519, 1989.
21. Grabau C and Cronan JE, Jr. *In vivo* function of *Escherichia coli* pyruvate oxidase specifically requires a functional lipid binding site. *Biochemistry* 25: 3748–3751, 1986.
22. Grabau C and Cronan JE, Jr. Molecular cloning of the gene (poxB) encoding the pyruvate oxidase of *Escherichia coli*, a lipid-activated enzyme. *J Bacteriol* 160: 1088–1092, 1984.
23. Grabbe R and Schmitz RA. Oxygen control of nif gene expression in *Klebsiella pneumoniae* depends on NifL reduction at the cytoplasmic membrane by electrons derived from the reduced quinone pool. *Eur J Biochem* 270: 1555–1566, 2003.
24. Gu D, Zhou Y, Kallhoff V, Baban B, Tanner JJ, and Becker DF. Identification and characterization of the DNA-binding domain of the multifunctional PutA flavoenzyme. *J Biol Chem* 279: 31171–31176, 2004.
25. Halouska S, Zhou Y, Becker DF, and Powers R. Solution structure of the *Pseudomonas putida* protein PpPutA45 and its DNA complex. *Proteins* 75: 12–27, 2009.
26. Hefti MH, Francoijs KJ, de Vries SC, Dixon R, and Vervoort J. The PAS fold. A redefinition of the PAS domain based upon structural prediction. *Eur J Biochem* 271: 1198–1208, 2004.
27. Heintzen C, Loros JJ, and Dunlap JC. The PAS protein VIVID defines a clock-associated feedback loop that represses light input, modulates gating, and regulates clock resetting. *Cell* 104: 453–464, 2001.
28. Hill S, Austin S, Eydmann T, Jones T, and Dixon R. *Azotobacter vinelandii* NIFL is a flavoprotein that modulates transcriptional activation of nitrogen-fixation genes via a redox-sensitive switch. *Proc Natl Acad Sci USA* 93: 2143–2148, 1996.
29. Key J, Hefti M, Purcell EB, and Moffat K. Structure of the redox sensor domain of *Azotobacter vinelandii* NifL at atomic resolution: Signaling, dimerization, and mechanism. *Biochemistry* 46: 3614–3623, 2007.
30. Koland JG, Miller MJ, and Gennis RB. Reconstitution of the membrane-bound, ubiquinone-dependent pyruvate oxidase respiratory chain of *Escherichia coli* with the cytochrome d terminal oxidase. *Biochemistry* 23: 445–453, 1984.
31. Kottke T, Hegemann P, Dick B, and Heberle J. The photochemistry of the light-, oxygen-, and voltage-sensitive domains in the algal blue light receptor phot. *Biopolymers* 82: 373–378, 2006.
32. Krishnan N and Becker DF. Characterization of a bifunctional PutA homologue from *Bradyrhizobium japonicum* and identification of an active site residue that modulates proline

reduction of the flavin adenine dinucleotide cofactor. *Biochemistry* 44: 9130–9139, 2005.
33. Lamb JS, Zoltowski BD, Pabit SA, Li L, Crane BR, and Pollack L. Illuminating solution responses of a LOV domain protein with photocoupled small-angle X-ray scattering. *J Mol Biol* 393: 909–919, 2009.
34. Larson JD, Jenkins JL, Schuermann JP, Zhou Y, Becker DF, and Tanner JJ. Crystal structures of the DNA-binding domain of *Escherichia coli* proline utilization. A flavoprotein and analysis of the role of Lys9 in DNA recognition. *Protein Sci* 15: 2630–2641, 2006.
35. Lee YH, Nadaraia S, Gu D, Becker DF, and Tanner JJ. Structure of the proline dehydrogenase domain of the multifunctional PutA flavoprotein. *Nat Struct Biol* 10: 109–114, 2003.
36. Linden H. Circadian rhythms. A white collar protein senses blue light. *Science* 297: 777–778, 2002.
37. Ling M, Allen SW, and Wood JM. Sequence analysis identifies the proline dehydrogenase and pyrroline-5-carboxylate dehydrogenase domains of the multifunctional *Escherichia coli* PutA protein. *J Mol Biol* 245: 950–956, 1994.
38. Little R, Martinez–Argudo I, and Dixon R. Role of the central region of NifL in conformational switches that regulate nitrogen fixation. *Biochem Soc T* 34: 162–164, 2006.
39. Liu Y, He Q, and Cheng P. Photoreception in *Neurospora*: A tale of two White Collar proteins. *Cell Mol Life Sci* 60: 2131–2138, 2003.
40. Losi A. Flavin-based Blue-Light photosensors: A photobiophysics update. *Photochem Photobiol* 83: 1283–1300, 2007.
41. Macheroux P, Hill S, Austin S, Eydmann T, Jones T, Kim S-O, Poole R, and Dixon R. Electron donation to the flavoprotein NifL, a redox-sensing transcriptional regulator. *Biochem J* 332: 413–419, 1998.
42. Marchal D, Pantigny J, Laval JM, Moiroux J, and Bourdillon C. Rate constants in two dimensions of electron transfer between pyruvate oxidase, a membrane enzyme, and ubiquinone (coenzyme Q8), its water-insoluble electron carrier. *Biochemistry* 40: 1248–1256, 2001.
43. Martinez–Argudo I, Little R, Shearer N, Johnson P, and Dixon R. The NifL–NifA system: A multidomain transcriptional regulatory complex that integrates environmental signals. *J Bacteriol* 186: 601–610, 2004.
44. Martinez–Argudo I, Little R, Shearer N, Johnson P, and Dixon R. Nitrogen fixation: Key genetic regulatory mechanisms. *Biochem Soc Trans* 33: 152–156, 2005.
45. Massey V. The chemical and biological versatility of riboflavin. *Biochem Soc Trans* 28: 283–296, 2000.
46. Mather MW and Gennis RB. Kinetic studies of the lipid-activated pyruvate oxidase flavoprotein of *Escherichia coli*. *J Biol Chem* 260: 16148–16155, 1985.
47. Menzel R and Roth J. Purification of the *put*A gene product. *J Biol Chem* 256: 9755–9761, 1981.
48. Moglich A and Moffat K. Structural basis for light-dependent signaling in the dimeric LOV domain of the photosensor YtvA. *J Mol Biol* 373: 112–126, 2007.
49. Muller YA and Schulz GE. Structure of the thiamine- and flavin-dependent enzyme pyruvate oxidase. *Science* 259: 965–967, 1993.
50. Neumann P, Weidner A, Pech A, Stubbs MT, and Tittmann K. Structural basis for membrane binding and catalytic activation of the peripheral membrane enzyme pyruvate oxidase from *Escherichia coli*. *Proc Natl Acad Sci USA* 105: 17390–17395, 2008.
51. Ostrovsky De Spicer P and Maloy S. PutA protein, a membrane-associated flavin dehydrogenase, acts as a redox-dependent transcriptional regulator. *Proc Natl Acad Sci USA* 90: 4295–4298, 1993.
52. Ostrovsky De Spicer P, O'Brian K, and Maloy S. Regulation of proline utilization in *Salmonella typhimurium*: A membrane-associated dehydrogenase binds DNA *in vitro*. *J Bacteriol* 173: 211–219, 1991.
53. Partch CL and Sancar A. Photochemistry and photobiology of cryptochrome blue-light photopigments: the search for a photocycle. *Photochem Photobiol* 81: 1291–1304, 2005.
54. Qi YN, Rao F, Luo Z, and Liang ZX. A flavin cofactor-binding PAS domain regulates c-di-GMP synthesis in AxDGC2 from *Acetobacter xylinum*. *Biochemistry* 48: 10275–10285, 2009.
55. Rebbapragada A, Johnson MS, Harding GP, Zuccarelli AJ, Fletcher HM, Zhulin IB, and Taylor BL. The Aer protein and the serine chemoreceptor Tsr independently sense intracellular energy levels and transduce oxygen, redox, and energy signals for *Escherichia coli* behavior. *Proc Natl Acad Sci USA* 94: 10541–10546, 1997.
56. Recny MA, Grabau C, Cronan JE, Jr., and Hager LP. Characterization of the alpha-peptide released upon protease activation of pyruvate oxidase. *J Biol Chem* 260: 14287–14291, 1985.
57. Recny MA and Hager LP. Isolation and characterization of the protease-activated form of pyruvate oxidase. Evidence for a conformational change in the environment of the flavin prosthetic group. *J Biol Chem* 258: 5189–5195, 1983.
58. Russell P, Hager LP, and Gennis RB. Characterization of the proteolytic activation of pyruvate oxidase. *J Biol Chem* 252: 7877–7882, 1977.
59. Russell P, Schrock HL, and Gennis RB. Lipid activation and protease activation of pyruvate oxidase. *J Biol Chem* 252: 7883–7887, 1977.
60. Scarpulla RC and Soffer RL. Membrane-bound proline dehydrogenase from *Escherichia coli*. *J Biol Chem* 253: 5997–6001, 1978.
61. Schreiner ME and Eikmanns BJ. Pyruvate:quinone oxidoreductase from *Corynebacterium glutamicum*: Purification and biochemical characterization. *J Bacteriol* 187: 862–871, 2005.
62. Schreiner ME, Riedel C, Holatko J, Patek M, and Eikmanns BJ. Pyruvate:quinone oxidoreductase in *Corynebacterium glutamicum*: Molecular analysis of the pqo gene, significance of the enzyme, and phylogenetic aspects. *J Bacteriol* 188: 1341–1350, 2006.
63. Schrock HL and Gennis RB. High affinity lipid binding sites on the peripheral membrane enzyme pyruvate oxidase. *J Biol Chem* 252: 5990–5995, 1977.
64. Schwerdtfeger C and Linden H. VIVID is a flavoprotein and serves as a fungal blue light photoreceptor for photoadaptation. *EMBO J* 22: 4846–4855, 2003.
65. Slavny P, Little R, Salinas P, Clarke TA, and Dixon R. Quaternary structure changes in a second Per-Arnt-Sim domain mediate intramolecular redox signal relay in the NifL regulatory protein. *Mol Microbiol* 75: 61–75, 2010.
66. Soderback E, Reyes–Ramirez F, Eydmann T, Austin S, Hill S, and Dixon R. The redox- and fixed nitrogen-responsive regulatory protein NIFL from *Azotobacter vinelandii* comprises discrete flavin and nucleotide-binding domains. *Mol Microbiol* 28: 179–192, 1998.
67. Sollner S, Schober M, Wagner A, Prem A, Lorkova L, Palfey BA, Groll M, and Macheroux P. Quinone reductase acts as a redox switch of the 20S yeast proteasome. *EMBO Rep* 10: 65–70, 2009.
68. Srivastava D, Schuermann JP, White TA, Krishnan N, Sanyal N, Hura GL, Tan A, Henzl MT, Becker DF, and Tanner JJ.

Crystal structure of the bifunctional proline utilization A flavoenzyme from *Bradyrhizobium japonicum*. *Proc Natl Acad Sci USA* 107: 2878–2883, 2010.
69. Srivastava D, Zhu W, Johnson WH, Jr., Whitman CP, Becker DF, and Tanner JJ. The structure of the proline utilization a proline dehydrogenase domain inactivated by N-propargylglycine provides insight into conformational changes induced by substrate binding and flavin reduction. *Biochemistry* 49: 560–569, 2010.
70. Surber MW and Maloy S. Regulation of flavin dehydrogenase compartmentalization: Requirements for PutA-membrane association in *Salmonella typhimurium*. *Biochim Biophys Acta* 1421: 5–18, 1999.
71. Tanner JJ. Structural biology of proline catabolism. *Amino Acids* 35: 719–730, 2008.
72. Taylor BL and Zhulin IB. PAS domains: Internal sensors of oxygen, redox potential, and light. *Microbiol Mol Biol Rev* 63: 479–506, 1999.
73. Thummer R, Klimmek O, and Schmitz RA. Biochemical studies of *Klebsiella pneumoniae* NifL reduction using reconstituted partial anaerobic respiratory chains of *Wolinella succinogenes*. *J Biol Chem* 282: 12517–12526, 2007.
74. Tittmann K, Golbik R, Ghisla S, and Hubner G. Mechanism of elementary catalytic steps of pyruvate oxidase from *Lactobacillus plantarum*. *Biochemistry* 39: 10747–10754, 2000.
75. Ukaegbu UE and Rosenzweig AC. Structure of the redox sensor domain of *Methylococcus capsulatus* (Bath) MmoS. *Biochemistry* 48: 2207–2215, 2009.
76. van der Horst MA and Hellingwerf KJ. Photoreceptor proteins, "star actors of modern times": A review of the functional dynamics in the structure of representative members of six different photoreceptor families. *Acc Chem Res* 37: 13–20, 2004.
77. Wang AY, Chang YY, and Cronan JE, Jr. Role of the tetrameric structure of *Escherichia coli* pyruvate oxidase in enzyme activation and lipid binding. *J Biol Chem* 266: 10959–10966, 1991.
78. Watts KJ, Johnson MS, and Taylor BL. Structure-function relationships in the HAMP and proximal signaling domains of the aerotaxis receptor Aer. *J Bacteriol* 190: 2118–2127, 2008.
79. Wille G, Meyer D, Steinmetz A, Hinze E, Golbik R, and Tittmann K. The catalytic cycle of a thiamin diphosphate enzyme examined by cryocrystallography. *Nat Chem Biol* 2: 324–328, 2006.
80. Wood J. Membrane association of proline dehydrogenase in *Escherichia coli* is redox dependent. *Proc Natl Acad Sci USA* 84: 373–377, 1987.
81. Zhang M, White TA, Schuermann JP, Baban BA, Becker DF, and Tanner JJ. Structures of the *Escherichia coli* PutA proline dehydrogenase domain in complex with competitive inhibitors. *Biochemistry* 43: 12539–12548, 2004.
82. Zhang TF and Hager LP. Binding of pyruvate oxidase alpha-peptide to phospholipid vesicles. *Arch Biochem Biophys* 255: 201–204, 1987.
83. Zhang W, Zhang M, Zhu W, Zhou Y, Wanduragala S, Rewinkel D, Tanner JJ, and Becker DF. Redox-induced changes in flavin structure and roles of flavin N(5) and the ribityl 2′-OH group in regulating PutA–membrane binding. *Biochemistry* 46: 483–491, 2007.
84. Zhang W, Zhou Y, and Becker DF. Regulation of PutA-membrane associations by flavin adenine dinucleotide reduction. *Biochemistry* 43: 13165–13174, 2004.
85. Zhou Y, Larson JD, Bottoms CA, Arturo EC, Henzl MT, Jenkins JL, Nix JC, Becker DF, and Tanner JJ. Structural basis of the transcriptional regulation of the proline utilization regulon by multifunctional PutA. *J Mol Biol* 381: 174–188, 2008.
86. Zhou Y, Zhu W, Bellur PS, Rewinkel D, and Becker DF. Direct linking of metabolism and gene expression in the proline utilization A protein from *Escherichia coli*. *Amino Acids* 35: 711–718, 2008.
87. Zhu W and Becker DF. Exploring the proline-dependent conformational change in the multifunctional PutA flavoprotein by tryptophan fluorescence spectroscopy. *Biochemistry* 44: 12297–12306, 2005.
88. Zhu W and Becker DF. Flavin redox state triggers conformational changes in the PutA protein from *Escherichia coli*. *Biochemistry* 42: 5469–5477, 2003.
89. Zoltowski BD and Crane BR. Light activation of the LOV protein vivid generates a rapidly exchanging dimer. *Biochemistry* 47: 7012–7019, 2008.
90. Zoltowski BD, Schwerdtfeger C, Widom J, Loros JJ, Bilwes AM, Dunlap JC, and Crane BR. Conformational switching in the fungal light sensor Vivid. *Science* 316: 1054–1057, 2007.
91. Zoltowski BD, Vaccaro B, and Crane BR. Mechanism-based tuning of a LOV domain photoreceptor. *Nat Chem Biol* 5: 827–834, 2009.

Address correspondence to:
Donald F. Becker
Department of Biochemistry
Beadle Center
University of Nebraska
Lincoln, NE 68588-0664

E-mail: dbecker3@unl.edu

Date of first submission to ARS Central, June 25, 2010; date of acceptance, July 10, 2010.

Abbreviations Used

BLUF = blue light sensing using flavin
FAD = flavin adenine dinucleotide
FMN = flavin mononucleotide
GHKL = gyrase
GSA = γ-glutamic acid semialdehyde
Hsp90 = histidine kinase, MutL
LOV = light, oxygen, and voltage
NAD^+ = nicotinamide adenine dinucleotide
P5C = Δ^1-pyrroline-5-carboxylate
P5CDH = P5C dehydrogenase
PAS = Per-Arnt-Sim
PDHC = pyruvate dehydrogenase complex
POX = pyruvate oxidase
PPG = *N*-propargylglycine
PQO = pyruvate:quinone oxidoreductase
PRODH = proline dehydrogenase
Put = proline utilization
RHH = ribbon-helix-helix
THFA = tetrahydro-2-furoic acid
TPP = thiamin pyrophosphate
VVD = vivid
WCC = white collar complex

This article has been cited by:

1. Lin Z. Li. 2012. Imaging mitochondrial redox potential and its possible link to tumor metastatic potential. *Journal of Bioenergetics and Biomembranes* . [CrossRef]
2. Richa Dhatwalia, Harkewal Singh, Michelle Oppenheimer, Pablo Sobrado, John J. Tanner. 2012. Crystal Structures of Trypanosoma cruzi UDP-Galactopyranose Mutase Implicate Flexibility of the Histidine Loop in Enzyme Activation. *Biochemistry* 120605103159006. [CrossRef]
3. Aba Losi, Wolfgang Gärtner. 2012. The Evolution of Flavin-Binding Photoreceptors: An Ancient Chromophore Serving Trendy Blue-Light Sensors. *Annual Review of Plant Biology* **63**:1, 49-72. [CrossRef]
4. Xiang Gao, Meng Qin, Puguang Yin, Junyi Liang, Jun Wang, Yi Cao, Wei Wang. 2012. Single-Molecule Experiments Reveal the Flexibility of a Per-ARNT-Sim Domain and the Kinetic Partitioning in the Unfolding Pathway under Force. *Biophysical Journal* **102**:9, 2149-2157. [CrossRef]
5. Michael A. Moxley, Donald F. Becker. 2011. Rapid Reaction Kinetics of Proline Dehydrogenase in the Multifunctional Proline Utilization A Protein. *Biochemistry* 111215082737002. [CrossRef]
6. Stephen W. Ragsdale , Li Yi . 2011. Thiol/Disulfide Redox Switches in the Regulation of Heme Binding to Proteins. *Antioxidants & Redox Signaling* **14**:6, 1039-1047. [Abstract] [Full Text HTML] [Full Text PDF] [Full Text PDF with Links]